# Paramagnetic States of Four Iron−Four Sulfur Clusters. 2. Proton ENDOR Study of a 1+ State in an Asymmetrical Cluster

**Laurent Le Pape,[†] Bernard Lamotte,* Jean-Marie Mouesca, and Gérard Rius[‡]**

*Contribution from the Département de Recherche Fondamentale sur la Matière Condensée, SCIB/SCPM, C.E.A./Grenoble, 17 rue des Martyrs, 38054 Grenoble Cedex 9, France*

*Received September 24, 1996. Revised Manuscript Received April 17, 1997[⊗]*

**Abstract:** Proton ENDOR spectroscopy on $\gamma$-irradiated single crystals of the synthetic model compound $(Et_4N)_2[Fe_4S_4(SC_6H_4\text{-}o\text{-}OH)_4]$ has been used to study a $[4Fe-4S]^+$ center that has properties similar to those of the reduced states of some particular ferredoxins and of the enzyme aconitase. The interesting point about this model compound is that one iron atom is five-coordinate, with an extra phenolic oxygen attached to one of its thiolate ligand. The complex thus represents an example of an asymmetrical [4Fe−4S] cluster in the solid crystalline state. From the study of the angular dependence of the proton ENDOR lines, it has been possible to derive eight hyperfine tensors of protons occupying different positions in the near vicinity of the iron atoms, the main bearers of the spin population of the paramagnetic anion. Some protons belong to thiolate ligands of the anion whereas others belong to close $(Et_4N)^+$ counterions. From the anisotropic parts of the tensors—and by using a multicentric point-dipole model—it has been possible to derive the distribution of the unpaired electron spin population on the different iron (and sulfur) atoms of the cluster. The spin populations thus obtained indicate that two iron atoms ($Fe_2$ and $Fe_3$) constitute a *localized* $Fe^{3+}-Fe^{2+}$ mixed-valence pair. Within the limitations of a *pairwise* vectorial spin coupling model that considers two iron pairs, these results show that the magnetic ground state of the center studied here most probably corresponds to a $|^9/_2,4,^1/_2\rangle$ spin state, where $^9/_2$, 4, and $^1/_2$ are the spin quantum numbers of the mixed-valence pair, the ferrous pair, and the cluster, respectively. Finally, it is found that the spin populations on the different iron atoms, obtained for this model system, are quite similar to those of reduced substrate-free aconitase derivable from previous Mössbauer and ENDOR measurements.

## Introduction

As shown in the preceding article, several $[4Fe-4S]^{3+}$ and $[4Fe-4S]^+$ paramagnetic centers have been identified and studied by EPR in $\gamma$-irradiated single crystals of the synthetic $(Et_4N)_2[Fe_4S_4(SC_6H_4\text{-}o\text{-}OH)_4]$ model compound.[1,2] Let us recall that the choice of this compound is not aimed at mimicing exactly the active site of any particular protein, but rather at treating a representative case of asymmetric cubane. The analysis of their **g**-tensors allowed us to assign each of them to one of the two expected oxidation states and, moreover, to suggest for most of the centers plausible localizations of their mixed-valence pairs. However, on the basis of the knowledge of their **g**-tensors alone, it is not possible to consider assignment of these locations as certain. Although good correlations have been found so far for (nearly) *symmetrical* compounds,[3] experimentally as well as theoretically, between the eigenvector $\mathbf{V}_1$ associated with the largest eigenvalue $g_1$ and the side of the cubane occupied by the mixed-valence pair, the situation is not as clear with the asymmetrical compound dealt with in the present two papers.

As far as the distribution of the unpaired spin population in the cluster is concerned, a previous study of a $[4Fe-4S]^{3+}$ paramagnetic center, made in single crystals of the $(Et_4N)_2[Fe_4S_4(SCH_2Ph)_4]$ compound has shown that this knowledge can be obtained by using proton ENDOR spectroscopy.[4] The spin population distribution can, in practice, be derived from an analysis of the anisotropic parts of the proton hyperfine tensors by the use of a multicenter point−dipole model.[4] The present article describes a similar study, made on the $[4Fe-4S]^+$ paramagnetic center called "center 8" (see the preceding paper). This center is characterized by the three following principal values of its **g**-tensor: $g_1 = 1.980$, $g_2 = 1.936$, and $g_3 = 1.825$. Two types of reasons have determined our choice to study this particular center by proton ENDOR. The first one is practical and is based on the fact that the EPR lines of center 8 are relatively intense, giving rise to ENDOR spectra of sufficient signal-to-noise ratio, and that they overlap minimally with the EPR lines of all the other paramagnetic species. The second one is that this center is especially interesting because, as discussed in the preceding paper, it was not possible to assign a location for its mixed-valence pair from the analysis of its **g**-tensor. Because of the spin−orbit coupling, the **g**-tensor of Fe(II) is much more sensitive to geometrical distortions than that of Fe(III) sites. The fifth coordination at a ferrous ion could therefore lead to such a tilt of the $g_1$ direction, especially in the $[4Fe-4S]^+$ redox state because it contains formally three Fe(II) and one Fe(III) ions. This work thus represents the first detailed and complete proton ENDOR study of a $[4Fe-4S]^+$ center in a single crystal, moreover for an asymmetric anion.

A Mössbauer study of the diamagnetic $(Et_4N)_2[Fe_4S_4(SC_6H_4\text{-}o\text{-}OH)_4]$ complex has shown that it did not have two well-delocalized mixed-valence pairs of the type $Fe^{2.5+}-Fe^{2.5+}$ as

[†] Presently at C.E.A./Grenoble, DRFMC/SCIB, laboratoire de Chimie de Coordination, Unité de Recherche Associée au CNRS No. 1194, 17 rue des Martyrs, 38054 Grenoble Cedex 9, France.

[‡] Presently at the Université de la Rochelle, Pôle Science et Technologie/LEMMA, Avenue Marillac, 17042 La Rochelle, France.

[⊗] Abstract published in *Advance ACS Abstracts,* September 15, 1997.

(1) Johnson, R. E.; Papaefthymiou, G. C.; Frankel, R. B.; Holm, R. H. *J. Am. Chem. Soc.* **1983**, *105*, 7280.

(2) Le Pape, L.; Lamotte, B.; Mouesca, J.-M.; Rius, G. *J. Am. Chem. Soc.* **1997**, *119*, 9757 (preceding paper in this issue).

(3) Gloux, J.; Gloux, P.; Lamotte, B.; Mouesca, J.-M.; Rius, G. *J. Am. Chem. Soc.* **1994**, *116*, 1953.

(4) Mouesca, J.-M.; Rius, G.; Lamotte, B. *J. Am. Chem. Soc.* **1993**, *115*, 4714.

S0002-7863(96)03350-1 CCC: $14.00 

observed for "classical" 2+ clusters (with usually $\delta \approx 0.46$ mm/s and $\Delta E_Q \approx 1.10$ mm/s), but rather one delocalized pair only (with $\delta = 0.48$ mm/s and $\Delta E_Q = 1.22$ mm/s) and one more or less localized $Fe^{3+}-Fe^{2+}$ pair (with $\delta = 0.43$ mm/s and $\Delta E_Q = 0.75$ mm/s and $\delta = 0.63$ mm/s and $\Delta E_Q = 1.84$ mm/s, respectively). This ferrous ion with $\delta = 0.63$ mm/s has been (tentatively) identified with $Fe_1$ by Johnson et al.[1] on the basis that $Fe_1$ is alone influenced by a secondary bonding interaction with an oxygen atom. It was of interest to learn whether, upon formation of center 8, this iron atom remained ferrous upon reduction of the cluster or whether it would belong to a delocalized $Fe^{2.5+}-Fe^{2.5+}$ pair.

## Experimental Section

**(1) Preparation of the $(Et_4N)_2[Fe_4S_4(SC_6H_4$-*o*-$OH)_4]$ Compound and of Crystal Samples.** Preparation of the $(Et_4N)_2[Fe_4S_4(SC_6H_4$-*o*-$OH)_4]$ compound (and of single crystals) has been described in the preceding article. A single crystal of about 10 mg was subsequently irradiated under argon atmosphere with a dose of 0.4 MGy of $\gamma$-rays in a $^{60}Co$ source at room temperature. Since the intensity of the EPR lines of the center 8 studied here decreased quite rapidly (over several days) after the irradiation, the oriented crystal was always kept at low temperatures in the spectrometer between the experiments, i.e., around 200 K, and at 10 K during the ENDOR measurements.

A previous study of the $(Et_4N)_2[Fe_4S_4(SCH_2Ph)_4]$ compound[4] had shown how much deuteration was required to avoid important overlaps of ENDOR lines (and thus greatly simplifying them). This is why we tried to prepare this compound, the subject of this paper, with deuterated counterions and selectively deuterated 2-mercaptophenol ligands. But we always failed to obtain crystals. Despite the mentioned difficulties, this study was thus performed with *fully* protonated crystals.

We postulate that our failure to obtain these deuterated crystals is related to the fact that the $(Et_4N)_2[Fe_4S_4(SC_6H_4$-*o*-$OH)_4]$ compound is only metastable in acetonitrile solution and tends to be transformed into a $(Et_4N)_2[Fe_2(SC_6H_4$-*o*-$O)_4]$ dinuclear sulfide-free $Fe_2$ cluster.[5] We observed, for the protonated compound, that this transformation becomes relatively rapid above 50 °C, and for this reason, the temperature of the acetonitrile solution was limited to this temperature during crystal growth. We suspect this maximum temperature to be somewhat lower for the deuterated compounds. In that case, either we kept the same conditions of growth for the deuterated crystals as those used for the protonated ones, and we obtained the dinuclear $Fe_2$ cluster, or we decreased this maximum temperature and the temperature gradient was not sufficient to grow single crystals. The crystallographic structure of the compound, published by Johnson et al.,[1] has been already described in the previous paper. The relative orientation of the crystal in the spectrometer is defined in such a way as to study the angular dependences of the ENDOR line positions in three perpendicular planes *a***b*, *bc*, and *ca**. This is also described in the preceding paper.

**(2) ENDOR Methodology.** The ENDOR experiments were performed on a BRUKER ER 200 D-SRC spectrometer equipped with the VARIAN E 1700 broad-band ENDOR accessory and a 100 W ENI 3100 L broad-band power amplifier. It was driven by a Hewlett-Packard computer HP 9153, through a homemade interface. For these experiments, the single crystals were kept at temperatures around 10 K in the spectrometer using an Oxford Instruments ESR-9 continuous flow helium cryostat. The ENDOR spectra were detected with amplitude modulation of the radio frequency at 12.5 kHz, without field modulation.

## Experimental Results

A typical proton ENDOR spectrum, obtained when the static magnetic field was set parallel to the *a** axis of the crystal, is presented in Figure 1. It exhibits relatively sharp lines and provides thus a good resolution. To follow the angular

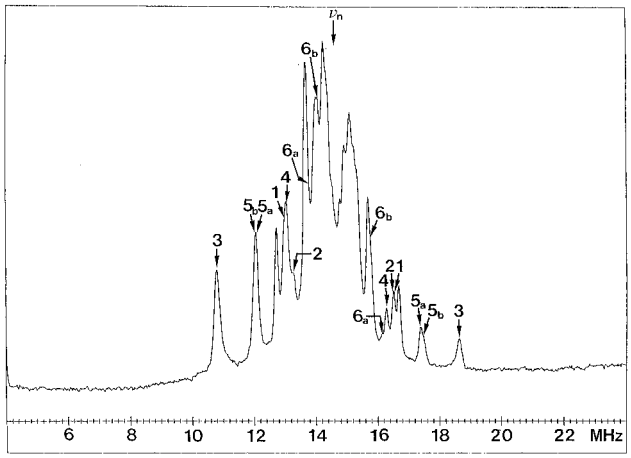


**Figure 1.** Proton ENDOR spectrum of center 8 obtained when the magnetic field is aligned along the *a** direction of the crystal defined in the text. Transitions are labeled according to the proton to which they are identified in the following of the text.

variations of the diverse ENDOR lines, similar spectra were taken each two degrees in the three orthogonal planes *a***b*, *bc*, and *ca**. For a given crystal orientation, an ENDOR spectrum has been obtained by sitting at the center of the EPR line corresponding to the paramagnetic center studied. In the two planes *a***b* and *bc*, the ENDOR spectra have been taken successively for the two EPR lines corresponding to the two different magnetic sites, called "A" and "B", and in an angular domain of 90° between these two axes. In the mirror plane *ca**, where these two sites become equivalent, they have been drawn over a range of 180°. These angular variations are shown in Figure 2a for the site A and in Figure 2b for the second site B. The different pairs of curves (associated with different protons) which could be completely followed in the three planes have been labeled from 1 to 6. For reasons which will be discussed below, two pairs of rather similar curves have been defined and called respectively (5a,b) and (6a,b).

All the curves are shown in these figures "for a fixed magnetic field", that is, after having reset each measured ENDOR frequency to a common value of the Zeeman proton frequency in order to mask (at least in part: see below) the effects of *g* anisotropy. We have encountered some difficulties in orienting our crystal with precision because its *b* and *c* axes do not correspond to crystal edges. Thus, we could only achieve a somewhat imperfect orientation of the crystal on the sample holder. Misorientation effects are particularly apparent when using ENDOR, due to the high resolution of this method. This effect is particularly visible for those protons in Figure 2a and Figure 2b having the largest and most anisotropic hyperfine tensors, as is for example the case for proton 1, in the mirror plane *ca**, close to the *c* axis. In the following calculations, and when the misorientation is apparent, only the average of the two transitions will be taken into account. The resulting loss of accuracy is insignificant because this relative misorientation can be estimated to be less than 2°.

Because it is difficult to follow the angular variations of transitions in the three perpendicular planes, particularly near the middle of the spectra, we have used a standard fitting procedure, in that we calculated the proton ENDOR transitions from the usual spin Hamiltonian:

$$H = \mathbf{S}\cdot\mathbf{A}\cdot\mathbf{I} - g_n\beta_n\mathbf{H}\cdot\mathbf{I} \qquad (1)$$

If the **g**-tensor were isotropic, the two ENDOR frequencies corresponding to the two possible nuclear transitions $|M_S,M_I\rangle$

(5) Le Pape, L.; Excoffon, P.; Lamotte, B.; Laugier, J.; Rius, G. *New. J. Chem.* **1997**, *21*, 231−235.

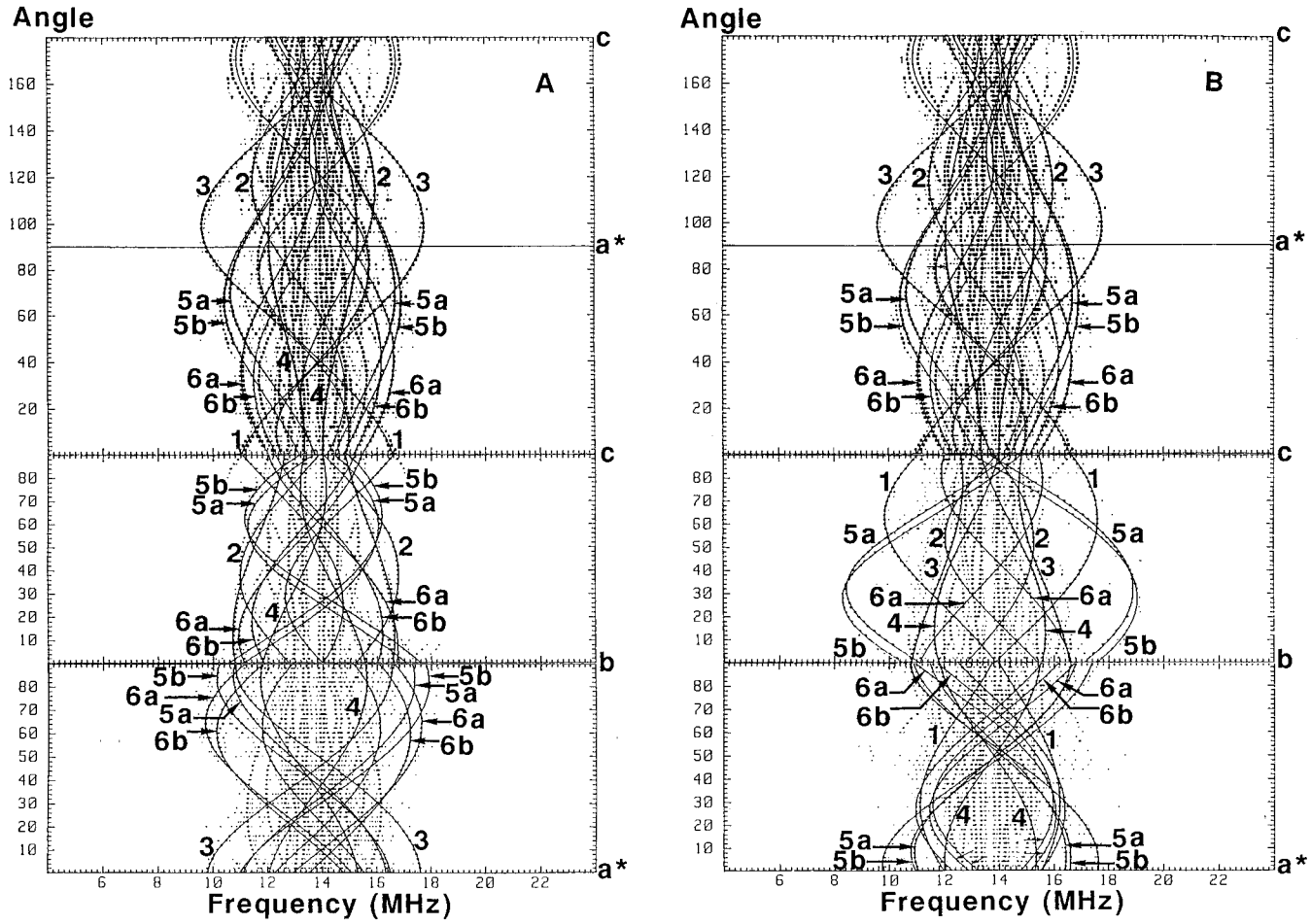


**Figure 2.** Angular dependences and fits (continuous lines) in the three orthogonal planes *a**b*, *bc*, and *ca** of the positions of the proton ENDOR lines. As indicated in the text, each measured ENDOR frequency has been reset to a common value $\nu_0$ of the Zeeman proton frequency (A) for "site A" and (B) for "site B".

$= |-^1/_2,+^1/_2\rangle \rightarrow |-^1/_2,-^1/_2\rangle$ and $|M_S,M_I\rangle = |+^1/_2,+^1/_2\rangle \rightarrow |+^1/_2,-^1/_2\rangle$ would be given by

$$\begin{cases} \nu^- = [\sum_{i=x,y,z} (^1/_2 \sum_{j=x,y,z} l_j A_{ij} + \nu_0 l_i)^2]^{1/2} \\ \nu^+ = [\sum_{i=x,y,z} (^1/_2 \sum_{j=x,y,z} l_j A_{ij} - \nu_0 l_i)^2]^{1/2} \end{cases} \quad (2)$$

In these last expressions, $\{A_{ij}\}$ are the tensorial elements of **A**, $\{l_i\}$ are the direction cosines of **H**, and $\nu_0$ is the transition frequency of far protons.

As shown in previous studies,[4,6] because of the small anisotropy of the **g**-tensor, the use of expressions eqs 1 and 2 was still sufficient, provided that we corrected the measured ENDOR frequencies for the nuclear Zeeman shift with the field, which was performed (as already stated above). Consequently, and in a given plane *i*, the ENDOR lines corresponding to one given proton were fitted by the following expression:

$$[\nu_i^{\pm}(\theta)]_{cor}{}^2 = U_i^{\pm} \cos^2\theta + V_i^{\pm} \sin^2\theta + 2W_i^{\pm} \sin\theta \cos\theta \quad (3)$$

It is then possible to extract from these fits, and for the three perpendicular planes, the corresponding components of the hyperfine **A** tensor. For example, for plane (*a**b*), one can use the following expression:

$$\begin{cases} A_{a^*a^*} = \dfrac{U^-_{a^*b} - U^+_{a^*b}}{2\nu_0} \\ A_{bb} = \dfrac{V^-_{a^*b} - V^+_{a^*b}}{2\nu_0} \\ A_{a^*b} = \dfrac{W^-_{a^*b} - W^+_{a^*b}}{2\nu_0} \end{cases} \quad (4)$$

The full hyperfine tensor for that proton, is thus given by

$$\mathbf{A} = \begin{pmatrix} \dfrac{U^-_{a^*b} - U^+_{a^*b}}{2\nu_0} & \dfrac{W^-_{a^*b} - W^+_{a^*b}}{2\nu_0} & \dfrac{W^-_{ca^*} - W^+_{ca^*}}{2\nu_0} \\ \dfrac{W^-_{a^*b} - W^+_{a^*b}}{2\nu_0} & \dfrac{U^-_{bc} - U^+_{bc}}{2\nu_0} & \dfrac{W^-_{bc} - W^+_{bc}}{2\nu_0} \\ \dfrac{W^-_{ca^*} - W^+_{ca^*}}{2\nu_0} & \dfrac{W^-_{bc} - W^+_{bc}}{2\nu_0} & \dfrac{U^-_{ca^*} - U^+_{ca^*}}{2\nu_0} \end{pmatrix} \quad (5)$$

In practice, a trial and error fitting procedure was followed for each proton. The first adjustments were made for the best experimentally determined portions of the curves of angular variations. Eight pairs of curves were thus obtained (shown in Figure 2A,B), from which eight hyperfine tensors were calculated. These tensors are those corresponding to the largest hyperfine couplings. Some portions of angular variation curves corresponding to other protons remained unfitted because it was not possible to follow them continuously in the three orthogonal planes *a**b*, *bc*, and *ca** (they disappeared close to the free proton resonance frequency due to overlaps with other lines). The complete hyperfine tensors were then diagonalized. In

(6) Atherton, N. M.; Horsewill, A. J. *Mol. Phys.* **1979**, *37*, 1349.

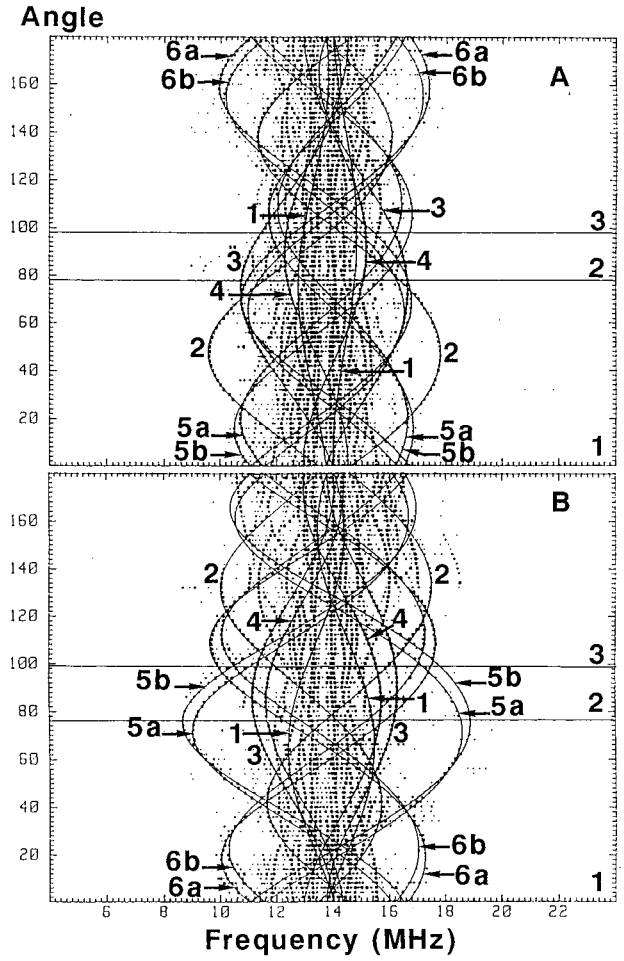


**Figure 3.** Angular dependences and fits (continuous lines), in the fourth plane defined in the text, of the positions of the proton ENDOR lines. As in Figure 2, each measured ENDOR frequency has been reset to a common value $\nu_0$ of the Zeeman proton frequency. Crossing directions of this fourth plane with *ca**, *bc*, and *a***b* planes are indicated by horizontal lines respectively labeled 1, 2, and 3 (A) for "site A" and (B) for "site B".

some cases, the relative sign ambiguity (due to a problem of continuity between two planes) is already lifted by EPR. As a matter of fact, the *a***c* plane is known, and in the *a***b* and *bc* planes, each site (A and B) can be separately followed to give the corresponding ENDOR angular variations.

To follow through, in the three planes, the curves belonging to each proton, a fourth plane was studied. This plane cuts the *a***b* plane at 14° of axis *b*, *bc* plane at 71° of axis *c*, and the *ca** plane at 43° of axis *c*. These two complementary angular variations are reported in Figure 3A,B. The verification consists of drawing, on these experimental figures, the curves of variation calculated from the hyperfine tensors deduced previously from the first three planes. As can be seen in Figure 3A,B, there is good agreement between experimental points and calculated curves.

The eight calculated hyperfine tensors are listed in Table 1. These tensors cannot be attributed as such to one of the two magnetic sites. Moreover, their global signs cannot yet be determined (this is a drawback of the ENDOR technique).

## Analysis of the Results

**(1) Introduction.** Each of the eight experimental hyperfine tensors was resolved into isotropic and anisotropic parts (see Table 1). It can be seen that, for each tensor, the isotropic contributions are much smaller than their respective anisotropic parts. Let us distinguish, however, between tensors 1 and 2 on one hand, whose isotropic values are small but definitely *nonzero*, and the six remaining tensors on the other hand (i.e., 3−6b), having negligible isotropic contributions (within experimental errors). The presence of a nonzero contact term is indicative of the presence of some spin density at the corresponding proton and, therefore, that this same proton most probably belongs to a thiolate of the paramagnetic anion.

**Table 1.** Eigenvalues (Complete Tensor, Isotropic, and Anisotropic Parts, in MHz) and Eigenvectors (Direction Cosines along the *a**, *b*, and *c* axes) of the Eight Measured Proton Hyperfine Tensors

| | eigenvalues | | | eigenvectors | | |
|---|---|---|---|---|---|---|
| tensor | total | iso | aniso | *a** | b | c |
| | −8.39 | | −7.76 | −0.23 | −0.48 | +0.85 |
| $\mathbf{A}_1$ | +5.18 | −0.64 | +5.82 | +0.86 | −0.51 | −0.06 |
| | +1.31 | | +1.94 | +0.46 | +0.71 | +0.53 |
| | +8.10 | | +8.28 | +0.39 | +0.74 | +0.54 |
| $\mathbf{A}_2$ | −5.49 | −0.18 | −5.31 | +0.89 | −0.44 | −0.03 |
| | −3.15 | | −2.97 | −0.22 | −0.50 | +0.84 |
| | +8.19 | | +8.26 | +0.99 | −0.03 | −0.16 |
| $\mathbf{A}_3$ | −6.04 | −0.07 | −5.97 | +0.07 | +0.97 | +0.25 |
| | −2.36 | | −2.29 | +0.15 | −0.25 | +0.96 |
| | +4.12 | | +4.18 | +0.10 | +0.97 | −0.23 |
| $\mathbf{A}_4$ | −3.39 | −0.06 | −3.34 | +0.98 | −0.14 | −0.15 |
| | −0.90 | | −0.84 | +0.17 | +0.21 | +0.96 |
| | +10.62 | | +10.60 | +0.13 | +0.84 | −0.53 |
| $\mathbf{A}_{5a}$ | −6.26 | +0.02 | −6.28 | +0.82 | +0.21 | +0.54 |
| | −4.30 | | −4.32 | −0.56 | +0.50 | +0.66 |
| | +11.00 | | +11.01 | +0.14 | +0.87 | −0.47 |
| $\mathbf{A}_{5b}$ | −6.71 | −0.02 | −6.69 | +0.81 | +0.16 | +0.56 |
| | −4.34 | | −4.32 | −0.56 | +0.46 | +0.69 |
| | +8.09 | | +8.09 | +0.43 | +0.90 | +0.01 |
| $\mathbf{A}_{6a}$ | −7.26 | ≈0 | −7.26 | +0.69 | −0.34 | +0.64 |
| | −0.82 | | −0.83 | −0.58 | +0.27 | +0.77 |
| | +7.25 | | +7.24 | +0.48 | +0.88 | +0.07 |
| $\mathbf{A}_{6b}$ | −7.01 | +0.01 | −7.02 | +0.66 | −0.41 | +0.63 |
| | −0.22 | | −0.22 | −0.58 | +0.25 | +0.77 |

The crystal structure of the anion reveals that there are at least four bonds (Fe−S−C−C−H being the shortest path) between a given iron atom and a proton (the possible exception being the OH proton "bonded" to $Fe_1$, in which case there would be only two bonds: Fe−O−H). This could in part explain why the isotropic couplings are so small. In constrast, for the $CH_2$ protons of the $[Fe_4S_4(SCH_2Ph)_4]^{1-}$ anion already studied in the same manner,[4] there were "only" three bonds to be considered (Fe−S−C−H). Moreover, the direct overlap existing between the s orbital of a given $CH_2$ proton and the polarized p orbital of the nearby organic sulfur provided much of the spin density at the level of the proton nucleus (equivalent to something like Fe−S···H). This is why the observed isotropic couplings were as high as 3.6 MHz.

Concerning the six other couplings (3−6b), all that can be said so far is that any proton attached to a molecule other than the paramagnetic one (diamagnetic anions or cations), even located in its vicinity, is expected to have negligible spin density on it and, therefore, no contact contribution to its hyperfine tensor. The reverse is not necessarily true: a traceless hyperfine tensor could still correspond to a proton of the paramagnetic center. We did not aim at analyzing these isotropic contributions quantitatively. However, the actual protons ultimately identified with the hyperfine tensors should be such as to comply with the two qualitative constraints commented on above.

**(2) Anisotropic Contributions.** Next we focus on the anisotropic parts of these tensors. First of all, we note that four tensors (5a,b and 6a,b) appear to be very similar in pairs (hence the notation adopted in Table 1). Their largest eigenvalues differ by 11% at most, and the corresponding eigenvectors are within

**Table 2.** Averaged Proton Hyperfine Tensors $\mathbf{A}_5$ and $\mathbf{A}_6$ Calculated before Diagonalization from Tensors $\mathbf{A}_{5a}$, $\mathbf{A}_{5b}$ and $\mathbf{A}_{6a}$, $\mathbf{A}_{6b}$, Respectively

| | eigenvalues | | | eigenvectors | | |
|---|---|---|---|---|---|---|
| tensor | total | iso | aniso | *a** | b | c |
| | +10.79 | | +10.79 | +0.14 | +0.86 | −0.49 |
| $\mathbf{A}_5$ | −6.47 | ≈0 | −6.47 | +0.81 | +0.18 | +0.54 |
| | −4.31 | | −4.31 | −0.56 | +0.48 | +0.68 |
| | +7.64 | | +7.64 | +0.45 | +0.89 | +0.04 |
| $\mathbf{A}_6$ | −7.11 | ≈0 | −7.11 | +0.68 | −0.37 | +0.63 |
| | −0.52 | | −0.52 | −0.58 | +0.26 | +0.77 |

4°. Most probably, each set of tensors (5a,b on one hand and 6a,b on the other hand) corresponds to two different, but very close, locations of the *same* proton. The origin of this duality will be sufficiently discussed at the end of this section, once the identification of the tensors has become clear. For the moment, we choose to average the two tensors of each set (by averaging their respective components in (*a**,*b*,*c*)), thus obtaining two "new" tensors (called 5 and 6, respectively) out of the four "old" ones; new tensors are presented in Table 2.

We further proceeded by identifying the six protons corresponding to the six hyperfine tensors 1−6. This could be achieved by the use of a multicenter point−dipole model developed previously by members of our group. This model[4] is somewhat similar to the "local site model" developed by Bertrand et al. for the simulation of magnetic interactions between paramagnetic prosthetic centers.[7] The anisotropic part of the hyperfine interaction has two contributing terms: the dipolar interaction between the electron spin (described by a normalized spin density function summing up to one for $S = {}^1/_2$) with the nuclear spin of interest (here a proton of nuclear spin $I = {}^1/_2$) and a "pseudo-dipolar" interaction related to the orbital magnetic momentum of the magnetic atom (here the iron atoms). A simple method (as far as the dipolar contribution is concerned) consists of describing the spin density function, defined at each point of the whole space surrounding the paramagnetic molecule of spin $^1/_2$, by a set of scalars located on the main bearers of that same density (in our case, the magnetic iron atoms and, through the delocalization process, the sulfur atoms). The details are discussed elsewhere.[4]

In this analysis, we will neglect the orbital contribution. It has already been shown that this was a good approximation in the case of a $[4Fe-4S]^{3+}$ cluster, formally comprising a mixed-valence pair and a ferric pair. Exactly following the very same reasoning, the same conclusion can be expected for reduced clusters. Equations 7 and 8 of Mouesca et al.[4] are still valid here: namely, for an iron−proton distance $R$ greater than 3 Å, the factor $\beta_e g_n \beta_n / R^3$ is less than 1.5 MHz. The only exception could be proton $H_1$ (belonging to a hydroxyl group), whose distance from $Fe_1$ is calculated to be between 1.38 and 3.01 Å. However, due to steric effects, it can be expected that this proton will lie at the farthest possible position from the iron (the upper limit of 3 Å being therefore reached): that this is actually the case will be shown below. This factor is further multiplied by local site $g_i$-tensors, whose elements are expected to be less than 0.1 (value estimated from the ferrous $g_i$-tensor of reduced rubredoxin). Finally, and for a given proton, contributions come essentially from one (or two) iron atoms (see Table 3). For all of these reasons, we decided not to take into account the orbital contribution, which is at most on the order of a few tenths of 1 MHz.

As a consequence, and within the multicenter point−dipole model, each measured anisotropic tensor is idealized as being a sum, in principle over all the atoms $i$ of the molecule, of "geometric" tensors $T[i,n]$ (that is, tensors involving only the relative coordinates of the atom $i$ and the proton nucleus $n$) weighted by scalars (spin populations $D_s[i]$):

$$T_{calc}[n] = \sum_i D_s[i]\, T[i,n] \tag{6}$$

We thus tried to find the optimal set of scalars $D_s[i]$ reproducing the experimentally measured tensors $T_{exp}[n]$, $n = 1-6$, by minimizing the following error function:

$$\mathrm{erf} = \sum_n \left[ \frac{T_{calc}[n] - T_{exp}[n]}{|T_{exp}[n]|_{max}} \right]^2 \tag{7}$$

The sum in eq 7 is performed over the individual components of the tensors, and $|T_{exp}[n]|_{max}$ is the largest eigenvalue in absolute value of the experimental tensor $T_{exp}[n]$. We define also the function err, which gives us an idea of the quality of the fit:

$$\mathrm{err} = \left( \frac{\mathrm{erf}}{n-p} \right)^{1/2} \tag{8}$$

where $n$ is the number of independent data we have at our disposal (five for each anisotropic tensor, hence 30 for the six hyperfine tensors) and $p$ is the number of *independent* parameters we use in a fitting procedure. This minimization procedure of course relies on the proper attribution of the tensors to the actual protons, and *both* the identification of the protons *and* the set of spin populations $\{D_s[i]\}$ are the outcomes of that search for the minimum of "erf" or "err".

Because the dipolar interaction varies as $r^{-3}$, we considered only the 13 protons located within 4 Å of an iron atom of the paramagnetic center; the six observed protons are listed in Table 3. They basically belong to two classes. The positions of most of the protons can namely be known from the crystal structure (for the determination of which their coordinates were introduced in the refinement procedure) and/or from direct calculations. Those are the CH groups of the ligand rings and the $CH_2$ groups of the cations. There are however protons whose exact positions is not known a priori: those are primarily the OH protons of the anions (the paramagnetic one, and possibly some of the neighboring molecules) and (to a lesser degree) the methyl groups $CH_3$ of the cations. The latter protons present only one degree of freedom, namely the rotation around the $C(H_2)-C(H_3)$ axis. The hydroxyl groups have, however, two such degrees: a rotation around the C−O(H) axis (defining an angle $\theta$; see Figure 4) and the C−O−H angle (the O−H distance was kept fixed to 0.96 Å as commonly observed by neutron diffraction for hydroxyl groups[8]).

**Table 3.** List of the Six Observed Protons and Corresponding Distances (Å) to the Iron Atoms (for OH Protons, Minimal, and Maximal Distances Are Reported)[a]

| | distance (Å) between proton and iron | | | |
|---|---|---|---|---|
| | $Fe_1$ | $Fe_2$ | $Fe_3$ | $Fe_4$ |
| H1 (OH) | **1.38/3.01** | 3.99/5.41 | 3.23/3.81 | 3.95/5.15 |
| H2 (OH) | 4.62/5.56 | **3.27/3.92** | 4.93/5.93 | 5.91/6.60 |
| H3 (CH) | 5.38 | 3.97 | **3.06** | 5.22 |
| H4 ($CH_2$) | 4.70 | 5.33 | **3.88** | 6.40 |
| H5 ($CH_2$) | 5.71 | **3.44** | 5.74 | 4.28 |
| H6 ($CH_2$) | 6.05 | 4.29 | 5.64 | **3.63** |

[a] The shortest distances are shown in bold type.

(7) Bertrand, P.; More, C.; Guigliarelli, B.; Fournel, A.; Bennett, B.; Howes, B. *J. Am. Chem. Soc.* **1994**, *116*, 3078.

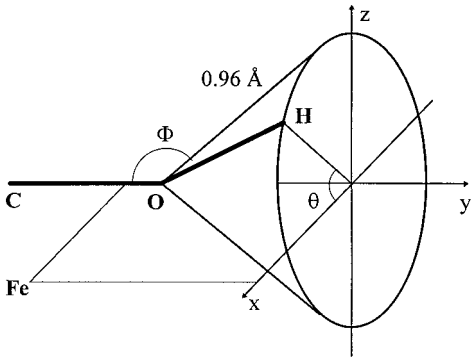


**Figure 4.** Scheme illustrating the method used to generate the different possible proton positions of the OH groups of the thiolate ligands.

Other unknowns of the problem are the absolute signs of the tensors. First, from an ENDOR experiment, only the magnitude of the hyperfine coupling is determined, but not its sign. Not known a priori are also the relative signs of $T_{exp}(a^*,b)$ and $T_{exp}(b,c)$ (two nondiagonal components of the experimental tensor $T_{exp}$) because we do not know which of the two magnetically equivalent sites we are observing. The first issue turns out to be a simple outcome of the whole process of identification of the protons seen by ENDOR, in parallel to the determination of the optimal set of spin population numbers. The expression of $T_{calc}[n]$ is linear in $D_s[i]$: obtaining the "best" set of $D_s[i]$'s yields the sign of $T_{calc}[n]$ (and of $T_{exp}[n]$, which $T_{calc}[n]$ is supposed to fit). On the second point, we notice that a change of the relative sign of $T_{exp}(a^*,b)$ and $T_{exp}(b,c)$ affects all the tensors at once (through their eigenvectors), and therefore, only two possibilities have to be considered (corresponding to the two possible sites). All the calculations were performed taking these two ambiguities into account and actually solve them in a clear-cut way.

We started the fitting procedure by considering at first spin densities only on the iron atoms (its main bearers, as already stated). For each of the six tensors, and going through the list of 13 selected protons, we determined the "best" set of spin populations, as well as the corresponding value of the function erf. We considered then sets of two, three, up to six, tensors, each time alternating the different signs involved. The assignments are not as difficult as it seems at first glance: even if the signs of all components of a tensor are not known, the eigenvector of the largest eigenvalue already gives a good idea about where the corresponding proton should be found. At the end of a series of trial and error tests, we had unambiguously identified the protons associated with the tensors 3−6 as being of the CH or $CH_2$ type (that is of fixed known positions): 3 is a CH proton of the ligand attached to $Fe_3$, 4 is a $CH_2$ proton of a vicinal cation, and 5 and 6 also belong to $CH_2$ groups but of another vicinal cation. The two remaining tensors 1 and 2 turned out to correspond to hydroxyl OH protons (those close to $Fe_1$ and $Fe_2$, respectively). One can verify that these assignments are compatible with the set of isotropic couplings measured for each of the protons: when definitely nonzero, for example (and within experimental error), they show that the corresponding protons surely belong to the paramagnetic anion (as is the case for $H_1$ and $H_2$).

With the assignments of tensors 3−6, we can follow in Figure 5 the variation of the value of the function err while moving each of the two OH protons (1 or 2) on their respective cone. For tensor 1, the minimum is well defined (around 170°), with an amplitude of variation of err of about 0.18, in contrast to tensor 2 (minimum around 300°) for which this amplitude is of "only" 0.04. This is due to the fact that $H_1$ (as defined in Table 3) is, on average, significantly closer than $H_2$ to any of the iron atoms (1.38−3.01 Å for the former to $Fe_1$, against 3.27−3.92 Å for the latter to $Fe_2$). The location of the six protons to which we assigned the six tensors are shown in Figure 6.

(8) Olovsson, I.; Jönsson, P.-G. *The Hydrogen Bond*; Olovsson, I., Jönsson, P.-G., Ed.; North-Holland Publishing Co.: Amsterdam, 1976; Vol. 2, pp 393−456.

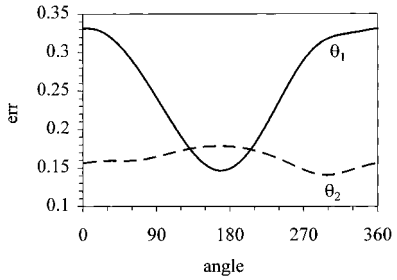


**Figure 5.** Variations as a function of the $\theta_i$ angle defined in Figure 4 of the err function (with $n = 25$ and $p = 4$) for the two $OH_i$ protons corresponding respectively to the tensors $\mathbf{A}_1$ and $\mathbf{A}_2$. We used fit #1b (four iron ions and normalized total spin population).

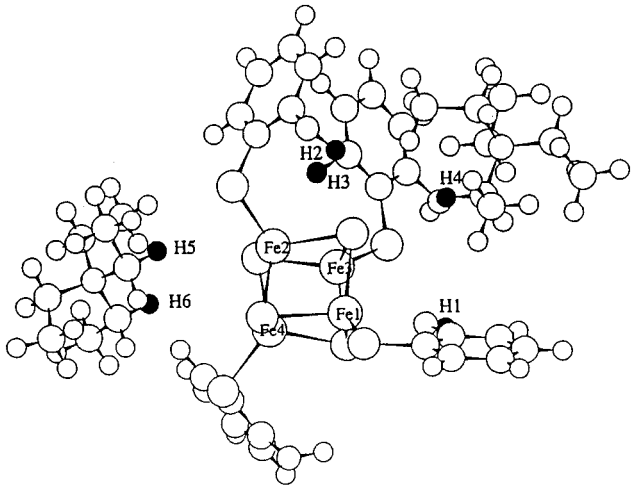


**Figure 6.** Representation of the position of the six protons (figured by black dots) attributed to the measured hyperfine tensors.

**Table 4.** Values of the Spin Populations as Obtained on the Iron Atoms[a]

| | steps | | | steps | |
|---|---|---|---|---|---|
| | #1a | #1b | | #1a | #1b |
| $D_s[Fe_1]$ | −1.42 | **−1.67** | $\theta_1$ (deg) | 156 | **168** |
| $D_s[Fe_2]$ | +3.03 | **+2.73** | $\theta_2$ (deg) | 301 | **313** |
| $D_s[Fe_3]$ | +1.25 | **+1.33** | Φ (deg) | 117 | **111** |
| $D_s[Fe_4]$ | −1.00 | **−1.39** | erf | 0.3590 | **0.5126** |
| $\sum D_s[i]$ | +1.86 | **+1.00** | err | 0.1249 | **0.1461** |
| | | | $p$ | 7 | 6 |

[a] There was no constraint for fit #1a. In fit #1b, the spin populations are normalized. Global spin populations, optimized angular parameters ($\theta_i$, $\varphi_i$) of the two OH protons, and erf and err functions defined in eqs 7 and 8, as well as the number $p$ of independent parameters are also given.

The spin population numbers obtained at this level of approximation (only the iron atoms were included in the minimization procedure) and the optimized values of the angular parameters characterizing the two OH protons are reported in the two columns of Table 4 (which differ in that the total spin population was, or was not, constrained to unity). Some comments are appropriate here before turning to refinements we made (that is, the inclusion of the sulfur atoms). First, we obtain two *positive* scalars for the spin densities located on iron 2 and 3. This allows us to identify them as belonging to the

mixed-valence pair. This assignment is possible because the total spin of the cluster is known to be aligned with the spin of this pair (whose two iron ions are ferromagnetically coupled to give, most probably, a dimer spin $^9/_2$ or $^7/_2$). Second, the two *negative* scalars of Fe sites 1 and 4 correspond to spin densities on the ferrous pair (with dimer spins 4 and 3, respectively). The change of sign indicates antiferromagnetic coupling of the spin of the ferrous pair to that of the mixed-valence pair, a coupling that results in a small value of the observed total spin, $S = {}^1/_2$. These results are consistent with the physical picture derived for the spin coupling properties of this type of $[4Fe-4S]^+$ cluster, and we will return to a more quantitative analysis of these scalars in the next section. We notice also that the spin densities are very large when compared to the experimental densities derived for an oxidized $[4Fe-4S]^{3+}$ cluster[4] or even to theoretical spin projection coefficients which these densities represent.[9] A similar observation holds for the unconstrained sum of the spin populations, equal to +1.86. This result, at this level of the fitting procedure, may let us suspect that something anomalous is happening. We will return to this point below, after having included the sulfur atoms into our search for an optimal spin population distribution.

We further refined the analysis by including the sulfur atoms. This was achieved in four steps. First, we included the sulfurs without any constraint at all, i.e., by fitting the data with 15 free parameters (i.e., four for the iron, eight for the organic and inorganic sulfur atoms, and three for the angular parameters of the OH protons). This fit, #2, provides a kind of "background" against which we can analyze more constrained models. The result of the unconstrained fit is presented in the first two columns of Table 5. The most striking feature of this trial concerns $Fe_4$ and its ligand (here $S_4$): its spin density drops from −1.00 (fit #1a, or −1.39 in fit #1b) to −0.34 (fit #2a, or −0.46 for fit #2b) while the density on the corresponding sulfur $S_4$ well exceeds those obtained for all the other sulfur atoms (organic or inorganic). This spin population $D(S_4)$ seems much too large if one considers that the main bearers of the spin population are the iron atoms and that the expected degree of delocalization cannot possibly be that high (for example, theoretical calculations predict that $D$(S) should be found around 5−10% of $D$(Fe) only). The spin populations of the inorganic sulfur atoms, however, assume quite reasonable values in this attempt.

This anomalous result (commented on below in relation with local displacements of the cation to which protons 5 and 6 belong) motivated other attempts to fit the data with more constrained models. Two (among others) types of constraints are possible (not mutually exclusive) and represented in eq 9a,b.

$$\begin{cases} D_s[S_i] = f_i \cdot D_s[Fe_i] & \text{(9a)} \\ D_s[S^*_i] = \sum_{j \neq 5-i} D_s[S_j] & \text{(9b)} \end{cases}$$

The first equation implies a common fraction of delocalization of the spin population from the iron atoms onto the ligand sulfur atoms (fraction $f$). This is meant to remedy the problem appearing at the level of $Fe_4$ and $S_4$. It is clear of course that one should have in principle one such scalar, $f_i$, for each type of iron ion: $Fe^{2+}$, $Fe^{3+}$, and $Fe^{2.5+}$. The scalars on the inorganic sulfur atoms are allowed to vary freely. The application of this first constraint results in the fit #3 in Table 5. Only fit #3b is acceptable (for fit #3a, $\sum D_s[i] = 2.22$, related to large $D_s$[S*]'s) and we obtain $f = 0.03$: this outcome is still consistent with both theoretical[10] and experimental[11] results, which predict (or measure) that the fraction of delocalization of the spin density from the irons to the sulfurs is a few percent.

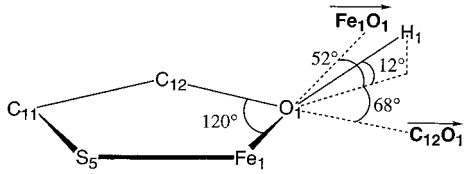


**Figure 7.** Scheme illustrating the optimized position of the proton $H_1$ obtained from step #5b of the fitting procedure.

Equation 9b assumes that an iron atom, to a first approximation, will have its spin density equally delocalized toward its four coordinated sulfurs (one "organic" and three "inorganic" ones). This approximation allowed us to deduce the amount of spin density on an inorganic sulfur $S^*_i$ from the fact that it is adjacent to three iron atoms, and will "receive" (so to speak) a contribution from each one, equal to that on the thiolate sulfur atom (see Figure 1 of Johnson et al.[1]) where $S^*_i$ is adjacent to the iron atoms $\{j = 1-4, j \neq 5 - i\}$. This is now fit #4 (a and b). When compared to fits #1−3, the density now calculated on $Fe_2$ is much larger. For fit #4a, $\sum D_s[i] = 1.75$ is still too large, whereas some of the densities $D_s$[S*]'s for fit #4b are also much too negative. Moreover, we still expect to find the same sign of the spin density on a given iron atom and its adjacent organic sulfur atom. Applying the whole set of constraints of eq 9 results in fit #5, of which #5b yields the same results as fit #1b (because $f$ is found to be zero).

We conclude this subsection with a comment about the local geometries obtained for the two OH protons, as seen by ENDOR. We can see at first that, from one fitting procedure to another, there is little variation in the values of the parameters $\theta_1$ and $\theta_2$: between 154° and 169° for $H_1$ and between 301° and 313° for $H_2$. We show in Figure 7 the optimized position of proton $H_1$, whose corresponding oxygen atom is weakly bonded to $Fe_1$: it adopts a location such that it lies in the plane $Fe_1-C-O_1$, the bond OH pointing to the *outside* of the pseudo-cycle $Fe_1-O_1-C-C-S_1$. This is readily understood by considering local steric effects which make the region inside the pseudo-cycle inaccessible. This can also explain why such an extreme position ($\theta_1 = 180°$ corresponds to the farthest position away from the iron) is not found for $H_2$, since this last proton belongs to a ligand whose oxygen is not bonded at all to any iron atom, as is the case for $H_1$.

**(3) On the Plausible Existence of a Small Local Counterion Displacement Due to a Vicinal Crystal Defect.** The spin densities of Tables 4 and 5 seem quite large to us. Since they have been calculated with the help of distances directly taken from the crystal structure of the $(Et_4N)_2[Fe_4S_4(SC_6H_4\text{-}o\text{-}OH)_4]$ compound, through the use of a point−dipole model implicating $(r_{Fe-H})^{-3}$, we can ask whether those distances are conserved for the paramagnetic center that we study. A first obvious fact is that the distances that we should use are in fact a little shorter than those we actually used because the X-ray study was done at room temperature while the ENDOR study was performed at 10 K. This effect, however, is not sufficient to cause such large spin densities on the iron atoms.

But there is another kind of difference that might eventually be important and that should now be discussed. During the previous EPR study of the paramagnetic centers in irradiated $(Et_4N)_2[Fe_4S_4(SCH_2Ph)_4]$ single crystals, it was found that some

(9) Mouesca, J.-M.; Noodleman, L.; Case, D. A. *J. Inorg. Biochem.* **1993**, *51*, 456.

(10) Mouesca, J.-M.; Chen, J. L.; Noodleman, L.; Bashford, D.; Case, D. A. *J. Am. Chem. Soc.* **1994**, *116*, 11898.

(11) Werst, M. M.; Kennedy, M. C.; Houseman, A. L. P.; Beinert, H.; Hoffman, B. M. *Biochemistry* **1990**, *29*, 10533.

**Table 5.** Values of the Spin Populations as Obtained on the Iron and Sulfur Atoms, Global Spin Populations, Fraction $f_i$ Defined in eq 9a, Optimized Angular Parameters ($\theta_i$, $\varphi_i$) of the Two OH Protons, erf and err Functions Defined in Eqs 7 and 8, and Number $p$ of Independent Parameters[a]

| | steps of the fitting procedure | | | | | | | |
|---|---|---|---|---|---|---|---|---|
| | #2a | #2b | #3a | #3b | #4a | #4b | #5a | #5b |
| $D_s[Fe_1]$ | −1.41 | −1.45 | −1.51 | **−1.81** | −1.39 | −1.50 | −1.34 | **−1.67** |
| $D_s[Fe_2]$ | +2.77 | +2.72 | +2.08 | **+2.54** | +3.28 | +3.43 | +2.85 | **+2.73** |
| $D_s[Fe_3]$ | +1.16 | +1.11 | +1.11 | **+1.27** | +1.01 | +1.16 | +1.21 | **+1.33** |
| $D_s[Fe_4]$ | −0.34 | −0.46 | −1.43 | **−1.46** | −0.71 | −0.55 | −0.95 | **−1.39** |
| $D_s[S^*_1]$ | +0.11 | +0.14 | +0.25 | **+0.13** | +0.14 | +0.02 | +0.08 | **+0.00** |
| $D_s[S^*_2]$ | −0.11 | +0.01 | +0.99 | **+0.14** | −0.36 | −0.59 | +0.02 | **+0.00** |
| $D_s[S^*_3]$ | +0.07 | +0.12 | +0.17 | **+0.14** | +0.07 | −0.08 | −0.03 | **+0.00** |
| $D_s[S^*_4]$ | −0.21 | −0.09 | +0.52 | **+0.03** | −0.18 | −0.51 | +0.09 | **+0.00** |
| $D_s[S_1]$ | −0.40 | −0.20 | −0.21 | **−0.05** | +0.07 | +0.12 | −0.04 | **+0.00** |
| $D_s[S_2]$ | −0.12 | −0.08 | +0.29 | **+0.08** | −0.18 | −0.31 | +0.09 | **+0.00** |
| $D_s[S_3]$ | +0.13 | +0.18 | +0.16 | **+0.04** | +0.25 | +0.21 | +0.04 | **+0.00** |
| $D_s[S_4]$ | −1.10 | −0.99 | −0.20 | **−0.04** | −0.26 | −0.41 | −0.03 | **+0.00** |
| $\sum D_s[i]$ | +0.56 | +1.00 | +2.22 | **+1.00** | +1.75 | +1.00 | +1.94 | **+1.00** |
| $f_i$ | | | 0.14 | **0.03** | | | 0.03 | **0.00** |
| $\theta_1$ (deg) | 156 | 156 | 156 | **169** | 155 | 154 | 154 | **168** |
| $\theta_2$ (deg) | 309 | 310 | 305 | **311** | 302 | 301 | 301 | **313** |
| $\Phi$ (deg) | 107 | 110 | 110 | **106** | 117 | 117 | 117 | **111** |
| erf | 0.0911 | 0.0950 | 0.2690 | **0.4975** | 0.2471 | 0.3507 | 0.3590 | **0.5126** |
| err | 0.0779 | 0.0771 | 0.1222 | **0.1618** | 0.1140 | 0.1324 | 0.1277 | **0.1493** |
| $p$ | 15 | 14 | 12 | **11** | 11 | 10 | 8 | **7** |

[a] Fit #2a has no constraint. Fit #3a uses eq 9a as an additional constraint. Fit #4a has eq 9b as a constraint. Fit #5a has been obtained by combining both constraints of eq 9. In Fits #b, the total spin populations are normalized to unity, in addition to the constraints already used in the corresponding fits #a.

of these species represented a variety of centers with slightly different **g**-tensors.[3] The same observation holds for the centers 6, 6′, and 6″ in the crystal of the compound studied here (see the preceding paper, Part 1). The different varieties found for the same center most probably correspond to the same geometrical disposition of the mixed-valence pair, but with slightly different local distortions in their immediate environment. This suggests that these centers have been trapped, at their creation, in the vicinity of a particular defect of the crystal structure and that they can occupy different sites close to this defect. Thus, this crystal defect will induce some structural distortion at the level of the paramagnetic center, the nature of the distortion being slightly different depending on the site that it occupies in the vicinity of the defect.

As a more general question, one could wonder why, upon $\gamma$-irradiation of a diamagnetic single crystal, several $[4Fe-4S]^+$ and $[4Fe-4S]^{3+}$ species are created, and not one species of each type. Our current explanation[3] suggests that the existence of these different centers is linked to different kinds of defects such as stacking faults and (or) dislocations in the crystal structure, the relative concentration of these defects varying certainly from one crystal to an other. This variability could well rationalize the observation that the different species do not have necessarily the same intensities when observed in different crystals. It is possible that some centers are in the immediate vicinity of the crystal fault and are thus rather strongly perturbed at one or two of their thiolate ligands, or the position of a counterion, while others may be a little more distant and thus only weakly (or not significantly) perturbed. Returning to the present ENDOR study of center 8, we observed two quite similar, but still different tensors 5a,b and 6a,b for protons 5 and 6, both pertaining to the same counterion. This might be a first indication of local moves of this counterion with respect to the $[4Fe-4S]^+$ cluster. It is in such a context that we wish to trace back the origin of the problems in our fitting procedures.

By comparing in Table 6 the experimental hyperfine tensors with those calculated (with the densities in column **5b** of Table 5), it is apparent that the largest eigenvalues are correctly estimated by the fit (to about ±10%), except for $H_6$, for which the calculated value (+5.03 MHz) is 35% less than the experimentally measured one (+7.64 MHz). We note also that the proton nearest to $Fe_4$ is that same $H_6$ ($d(H_6-Fe_4) = 3.63$ Å whereas $d(H_6-S_4) = 3.35$ Å). It seems as if by keeping the positions of the protons in the crystal structure as they are, the fit tends to artificially increase the spin density at the level of $S_4$ to compensate for the most probable situation that $H_6$ is actually closer to $Fe_4$ and $S_4$ for the $[4Fe-4S]^+$ cluster than it

**Table 6.** Comparison between Calculated and Experimental Hyperfine Anisotropic Tensors (MHz)

| | | exp | calc | exp | calc | exp | calc |
|---|---|---|---|---|---|---|---|
| | principal value | −7.76 | −8.78 | +5.82 | +6.60 | +1.94 | +2.18 |
| $H_1$ | $a^*$ (deg) | 103 | 104 | 31 | 30 | 63 | 64 |
| | $b$ (deg) | 119 | 125 | 121 | 119 | 44 | 49 |
| | $c$ (deg) | 32 | 39 | 93 | 96 | 58 | 52 |
| | angular shift (deg) | 7 | | 3 | | 6 | |
| | principal value | +8.28 | +8.37 | −5.31 | −5.15 | −2.97 | −3.22 |
| $H_2$ | $a^*$ (deg) | 67 | 69 | 26 | 36 | 103 | 118 |
| | $b$ (deg) | 42 | 35 | 116 | 121 | 120 | 106 |
| | $c$ (deg) | 57 | 63 | 92 | 74 | 33 | 33 |
| | angular shift (deg) | 7 | | 19 | | 19 | |
| | principal value | +8.26 | +8.53 | −5.97 | −5.85 | −2.29 | −2.68 |
| $H_3$ | $a^*$ (deg) | 10 | 15 | 86 | 90 | 81 | 75 |
| | $b$ (deg) | 92 | 86 | 15 | 12 | 105 | 102 |
| | $c$ (deg) | 99 | 105 | 76 | 78 | 17 | 20 |
| | angular shift (deg) | 8 | | 5 | | 7 | |
| | principal value | +4.18 | +4.08 | −3.34 | −3.12 | −0.84 | −0.96 |
| $H_4$ | $a^*$ (deg) | 84 | 84 | 11 | 14 | 80 | 77 |
| | $b$ (deg) | 15 | 15 | 98 | 99 | 78 | 78 |
| | $c$ (deg) | 103 | 104 | 98 | 101 | 16 | 18 |
| | angular shift (deg) | 1 | | 3 | | 3 | |
| | principal value | +10.79 | +9.67 | −6.48 | −5.83 | −4.31 | −3.84 |
| $H_5$ | $a^*$ (deg) | 82 | 76 | 35 | 43 | 124 | 130 |
| | $b$ (deg) | 31 | 33 | 80 | 80 | 61 | 59 |
| | $c$ (deg) | 120 | 119 | 57 | 48 | 47 | 55 |
| | angular shift (deg) | 6 | | 9 | | 8 | |
| | principal value | +7.64 | +5.03 | −7.12 | −4.71 | −0.53 | −0.32 |
| $H_6$ | $a^*$ (deg) | 63 | 59 | 47 | 57 | 125 | 131 |
| | $b$ (deg) | 27 | 34 | 112 | 121 | 75 | 77 |
| | $c$ (deg) | 88 | 78 | 51 | 49 | 39 | 44 |
| | angular shift (deg) | 11 | | 11 | | 6 | |

**Table 7.** Contribution of the Different Protons to the Error Function erf, with Six, Five, or Four Protons Included in the Fitting Procedure #1b (Four Iron Spin Populations and Normalized Total Spin Population)

| no. of H | contribution to the error function "erf" (%) | | | | | |
|---|---|---|---|---|---|---|
| | $H_1$ | $H_2$ | $H_3$ | $H_4$ | $H_5$ | $H_6$ |
| six | 11 | 12 | 07 | 01 | 09 | **59** |
| five | 18 | 20 | 11 | 11 | **38** | |
| four | 23 | 24 | 19 | 34 | | |

**Table 8.** Values of the Spin Populations on the Iron and Sulfur Atoms When Including Only Five or Four Protons (with Fits #1a (Four Iron Ions) and #1b (four Iron Ions) with Normalized Total Spin Populations)[a]

| | five protons | | four protons | |
|---|---|---|---|---|
| | #1a | #1b | #1a | #1b |
| $D_s[Fe_1]$ | −1.35 | −1.39 | −1.41 | −1.41 |
| $D_s[Fe_2]$ | +2.61 | +2.53 | +2.19 | +2.19 |
| $D_s[Fe_3]$ | +1.32 | +1.40 | +1.40 | +1.42 |
| $D_s[Fe_4]$ | −1.10 | −1.54 | −1.03 | −1.20 |
| $\sum D_s[i]$ | +1.48 | +1.00 | +1.14 | +1.00 |
| $\theta_1$ (deg) | 156 | 160 | 160 | 161 |
| $\theta_2$ (deg) | 321 | 327 | 338 | 339 |
| $\Phi$ (deg) | 117 | 115 | 113 | 113 |
| erf | 0.1559 | 0.1746 | 0.0880 | 0.0889 |
| err | 0.0931 | 0.0959 | 0.0823 | 0.0797 |
| $p$ | 7 | 6 | 7 | 6 |

[a] Also given are the total spin populations, the optimized angular parameters ($\theta_i$, $\varphi_i$) of the two OH protons, and the err and erf functions (cf. eqs 7 and 8) as well as the number $p$ of independent parameters.

is for the original $[4Fe-4S]^{2+}$ clusters belonging to the diamagnetic crystal matrix. It can be verified that, to a lesser degree, the same argument could be made for $H_5$ (with a calculated largest eigenvalue of +9.67 MHz versus +10.79 MHz experimentally measured, that is, a reduction by 10%). We can correlate this apparent defect of the fitting procedure with two observations: first, both protons $H_5$ and $H_6$ belong to the *same* cation, which is actually the closest to the paramagnetic anion, and second, the actual measured tensors for $H_5$ and $H_6$ appeared in pairs ($\mathbf{A}_{5a}-\mathbf{A}_{5b}$) and ($\mathbf{A}_{6a}-\mathbf{A}_{6b}$). This strongly supports the idea that, upon creation of the paramagnetic center 8 in the vicinity of a crystal defect, the closest of the cations is induced to come somewhat closer to that center (while adopting two slightly different positions).

We can test this hypothesis in the following way. If one considers in the first line of Table 7 the different contributions to the value of the error function erf, one notices that, at the level of the fit #1b for example (involving only the iron atoms), the tensor $\mathbf{A}_6$ accounts for 59% of the error made. It can be verified that the eigenvalues, but not the eigenvectors, are affected. We proceeded therefore, to another fit (fit #1b, but removing this tensor 6) to see what effect this has on the spin densities and on the distribution of the contributions to erf. This is presented in Tables 7 and 8: the mean densities for each pair decrease, and the tensor $\mathbf{A}_5$ is now found to contribute the most to the error of the fit (by 38%, whereas the average error for five protons should be around 20% if the error were evenly distributed). Finally, we also removed this tensor $\mathbf{A}_5$ from the fitting procedure: the spin densities dropped once more, but the partition of the error is now made approximately equal. Moreover, without the constraint on the total density (fit #1a), this sum decreases regularly down to +1.14, which is a quite reasonable value.

Interestingly, the two protons to present singular behaviors are shown by this series of calculations to be $H_5$ and $H_6$. It can be argued therefore that, upon formation of center 8, the whole cation bearing the two protons $H_5$ and $H_6$ must have moved closer to the paramagnetic anion. We can roughly evaluate this shortening by noticing that the largest of the eigenvalues of a hyperfine tensor is mainly proportional to the inverse cube of the distance between the proton and the ion bearing the spin density. A rough estimate of the *actual* distance $d(H_6)_{para}$ between $H_6$ and the paramagnetic cluster $[4Fe-4S]^+$ (that is $Fe_4$, after Table 3), compared to the same distance in the diamagnetic $[4Fe-4S]^{2+}$ matrix ($d(H_6)_{dia} = 3.63$ Å) results in a shortening by 13% upon reduction (from $[7.64/5.03] \approx 1.52 \approx [1.15]^3 \approx [d(H_6)_{dia}/d(H_6)_{para}]^3$, that is $d(H_6)_{para} \approx 3.16$ Å or a shortening by ca. 0.47 Å). Such a shortening can be related also to the fact that, upon reduction, the negative charge of the anion increases from −2 to −3, thus attracting the nearest cation $(Et_4N)^+$ more strongly.

**Table 9.** Comparison between the Calculated and Crystallographic Positions of the Protons $H_1-H_{6b}$ Using the Spin Populations of Fit #1b (Four Iron Ions with Normalized Total Spin Population) Obtained for the Four Protons $H_1-H_4$ (cf. Table 7)[a]

| | $H_1$ OH | $H_2$ OH | $H_3$ CH | $H_4$ $CH_2$ | $H_{5a}$ $CH_2$ | $H_{5b}$ $CH_2$ | $H_{6a}$ $CH_2$ | $H_{6b}$ $CH_2$ |
|---|---|---|---|---|---|---|---|---|
| $r_{cryst}$ | 4.08 | 4.68 | 4.18 | 4.87 | 4.59 | 4.59 | 4.70 | 4.70 |
| $r_{calc}$ | 4.05 | 4.54 | 4.12 | 4.83 | 4.35 | 4.27 | 4.11 | 4.15 |
| $\theta_{cryst}$ (deg) | +32 | −40 | +12 | +18 | −47 | −47 | −19 | −19 |
| $\theta_{calc}$ (deg) | +35 | −44 | +9 | +20 | −47 | −45 | −25 | −22 |
| $\Phi_{cryst}$ (deg) | 289 | 224 | 184 | 237 | 99 | 99 | 88 | 88 |
| $\Phi_{calc}$ (deg) | 292 | 220 | 180 | 239 | 106 | 106 | 94 | 93 |
| $d_{min}$ | 0.23 | 0.17 | 0.29 | 0.26 | 0.46 | 0.50 | 0.84 | 0.67 |
| erf($10^{-4}$) | 69 | 63 | 18 | 156 | 4 | 6 | 92 | 116 |

[a] For protons $H_1$ and $H_2$, "crystallographic" positions are in fact those derived from the same fitting step #1b just mentionned.

To get a more quantitative estimate of this displacement (somewhat more precise than the crude estimate mentionned just above), we present here a last series of calculations. Starting from a given set of spin populations (that of fit #1b with four protons; see Table 8), we can localize, for each of the 8 experimental tensors (from $\mathbf{A}_1$ to $\mathbf{A}_{6b}$), the optimized (in the sense of lowest erf values) positions of the corresponding protons. Each of them is located by its spherical coordinates $(r,\theta,\Phi)$ in $(a^*,b,c)$ with the center of the cubane as the origin. The results are presented in Table 9. As can be seen, the average $d_{min}$ value (distance between calculated and crystallographic positions) for the first four protons is 0.24 Å versus 0.48 Å for proton $H_5$ and 0.76 Å for proton $H_6$ (such an agreement is obviously expected for the first four protons since the densities used here were determined by their corresponding tensors). The values are to be correlated with those of the differences ($r_{cryst} - r_{calc}$): 0.07 Å in average for $H_1-H_4$ but 0.28 Å for $H_5$ and 0.57 Å for $H_6$. If we finally calculate the hyperfine tensors for $H_5$ and $H_6$ at these optimized positions, we obtain for the largest principal value +8.04 and +7.28 MHz, respectively, versus +8.08 and +7.24 MHz experimentally.

**(4) Analysis of the Spin Populations.** To obtain knowledge about the electronic structure of the paramagnetic center as described by the set of scalars we obtained on the iron and sulfur atoms, it is useful to have a proper understanding of what those numbers actually are. A detailed discussion on that subject has already been given elsewhere for a $[4Fe-4S]^{3+}$ center.[4] We therefore summarize here the main conclusions of that discussion. The scalars found by our analysis of the anisotropic parts of the hyperfine tensors are interpreted as being the spin populations on those iron atoms. Within the framework of the valence-bond model (ascribing spin populations only to the magnetic iron atoms, or, equivalently, not allowing delocalization processes to occur between the iron and the sulfur atoms), those spin populations $D_s[Fe_i]$ are nothing but spin coupling

**Table 10.** Spin Coupling Coefficients $\{K_i\}$ Compared with the "Experimental" Spin Populations Derived from Fits #1b (Four Iron Ions with Normalized Total Spin Population) Using Six and Four Protons

| | localized pair | | | delocalized pair | |
|---|---|---|---|---|---|
| | $K_2$ | $K_3$ | $K_1 = K_4$ | $K_2 = K_3$ | $K_1 = K_4$ |
| $\|^9/_2,4,^1/_2\rangle$ | +2.04 | +1.63 | −1.33 | +1.83 | −1.33 |
| $\|^7/_2,3,^1/_2\rangle$ | +1.76 | +1.24 | −1.00 | +1.50 | −1.00 |
| $\|^5/_2,2,^1/_2\rangle$ | +1.53 | +0.80 | −0.67 | +1.17 | −0.67 |
| | $D_s[Fe_2]$ | $D_s[Fe_3]$ | $D_s[Fe_1]/D_s[Fe_4]$ | $D_s[Fe_2] = D_s[Fe_3]$ | $D_s[Fe_1] = D_s[Fe_4]$ |
| with six H | +2.73 | +1.33 | −1.67/−1.39 | +2.03 | −1.53 |
| with four H | +2.19 | +1.42 | −1.41/−1.20 | +1.81 | −1.31 |

coefficients $\{K_i\}$ corresponding to a given spin state of the cluster. One can write such a spin state as following: $|S_{mv},S_{ferrous},S_{total}\rangle$, where $S_{mv}$ (ranging from $^1/_2$ to $^9/_2$, for $[4Fe-4S]^+$), $S_{ferrous}$ (ranging from 0 to 4), and $S_{total}$ (from $^1/_2$ to 17/2) are the spin quantum numbers of the mixed-valence pair, the ferrous pair, and the cluster, respectively. Among all the possible spin states, three are to be considered: $|^9/_2,4,^1/_2\rangle$, $|^7/_2,3,^1/_2\rangle$, and $|^5/_2,2,^1/_2\rangle$. For each of them, there are two possibilities: the mixed-valence pair is either delocalized or localized.

The spin coupling coefficients corresponding to the three spin states for the two situations are given in Table 10, where they are compared to the experimentally determined spin population numbers obtained when fitting the data with six and four protons (see Tables 4 and 8). This comparison leads to the following conclusions. First, the mixed-valence pair is localized, that is $Fe_2$ is a $Fe^{3+}$ ion whereas $Fe_3$ is a $Fe^{2+}$ ion. This result is in contrast to the case of the same pair in the compound $[Fe_4S_4(SCH_2Ph)_4]^{3+}$, where it appeared as delocalized. We note already that neither of the two iron atoms 2 or 3 is coordinated to an oxygen atom (as is the case for iron 1). The origin of the localization process has therefore to be found elsewhere (possibly in the existence of the local distortion involving the counterion displacement discussed above). Second, the spin population magnitudes are so large as to be compatible only with the spin state of the largest pair spins, that is the state $|^9/_2,4,^1/_2\rangle$. Moreover, the comparison of the magnitudes (averaged or not) of the spin coupling coefficients for that state with the experimental spin populations also supports the idea that the nearest cation to the paramagnetic anion has come closer upon electron capture of the center. One can verify namely that the densities obtained from the four protons 1−4 are smaller than those obtained from the six original protons, and in much better agreement with the theoretical spin coupling coefficients expected for the state $|^9/_2,4,^1/_2\rangle$.

It is now interesting to compare these results with the spin populations and/or spin states for other clusters. Let us start our discussion with the $[4Fe-4S]^{3+}$ state. As mentioned already, only one other paramagnetic center has been fully studied in much the same way as the one in this paper. For the center IV in $(Et_4N)_2[Fe_4S_4(SCH_2Ph)_4]$, it was found that the proper spin state describing the system was $|^7/_2,3,^1/_2\rangle$. Moreover, the mixed-valence pair appeared as delocalized. Such an analogous study was performed also on other oxidized centers named I[4,12] and III.[12] In the first case, the spin densities were found to be higher than in center IV, substantially distinct on the mixed-valence pair, and leading to an identification of that state as being $|^9/_2,4,^1/_2\rangle$.[4] For center III, the spin densities are comparable as those found for center IV on the mixed-valence pair. In describing protein active sites, an analysis of the $^{57}Fe$ isotropic hyperfine couplings measured by Mössbauer in "classical" HiPIP centers, within a general framework including 1Fe, 2Fe, 3Fe, and 4Fe clusters, lead members of our group to identify their spin state as being $|^7/_2,3,^1/_2\rangle$.[13]

Turning now to the $[4Fe-4S]^+$ state, the mixed-valence pair of center $I_R$[12] in the $(Et_4N)_2[Fe_4S_4(SCH_2Ph)_4]$ compound appeared as rather delocalized: the spin state is, most probably, $|^7/_2,3,^1/_2\rangle$. The same analysis as that mentioned above,[13] conducted on the aconitase system, led to an identification of that spin state as being $|^9/_2,4,^1/_2\rangle$.[13] In this last case, the point of interest lies in that the cluster presents an asymmetry due to one iron atom being coordinated to three sulfur and 2 (or 3) oxygen atoms. In the same piece of work,[13] "classical" reduced [4Fe−4S] ferredoxin centers, are instead described by the spin state $|^7/_2,3,^1/_2\rangle$. The whole set of data is presented in Table 11.

We thus observe the interplay of four factors: the redox state of the cluster, possible asymmetries induced by the crystalline (or proteinic) environment and/or by chemical differentiation of an iron site (extra coordination), mixed-valence pairs being anything from fully localized to fully delocalized, and the resulting spin state: $|^9/_2,4,^1/_2\rangle$ versus $|^7/_2,3,^1/_2\rangle$. The magnetic description of the clusters, as obtained from our spectroscopic studies, allow us to construct a database. This is a prerequisite for an understanding of the link between structural features (geometry, chemistry, environment, etc.) and magnetic coupling of the iron spins.

For example, "symmetrical" HiPIP/ferredoxin centers seem to systematically present a *delocalized* $|^7/_2,3,^1/_2\rangle$ spin state. Does this mean for certain that the (spectroscopic) measurement of a $|^9/_2,4,^1/_2\rangle$ state (localized or delocalized) is indicative of some perturbation of the cubane, as for center I, aconitase, and, in this paper, centers 8 and 9? Such a correlation, if substantiated, could be very interesting and the ability to distinguish between $|^9/_2,4,^1/_2\rangle$ and $|^7/_2,3,^1/_2\rangle$ spin states then matters a great deal. Subtle effects would have to be taken into account (site asymmetries, multiple super-J/double-B exchange terms, etc.) to develop a phenomenological model dealing with these questions. But such a work is beyond the scope of this paper.

## Conclusion

We have reported here ENDOR measurements of the hyperfine tensors of protons located in the close vicinity of a reduced $[4Fe-4S]^+$ cluster, created by $\gamma$-irradiation of the compound $(Et_4N)_2[Fe_4S_4(SC_6H_4\text{-}o\text{-}OH)_4]$. The choice of that compound was motivated by the fact that one of the four OH groups of the thiolate ligands has its oxygen atom weakly bonded to its corresponding iron atom (with $d(Fe_1-O) \approx 2.32$Å). This provided us with an asymmetrical-type of cluster in which one of the four iron atoms was differentiated from the three others. This is in constrast to a previous study of the same kind, performed on a (nearly) symmetrical compound.[4] It has not been possible, in the present case, to exploit much the isotropic hyperfine coupling constants, as was previously done for the other compound.[4] But, within the multicentric point−dipole approximation, it has been possible to identify in the crystal structure six protons for which we measured the hyperfine tensors and simultaneously to estimate the distribution of the spin population on the iron atoms of the $[4Fe-4S]^+$ core. Comparison of these experimentally determined spin populations with theoretical spin coupling coefficients allowed us to identify

(12) Noodleman, L.; Chen, J. L.; Case, D. A.; Giori, C.; Rius, G.; Mouesca, J.-M.; Lamotte, B. *Nuclear Magnetic Resonance of Paramagnetic Macromolecules*; La Mar, G. N., Ed.; Kluwer Academic Publishers: Dordrect, The Netherlands, 1995; pp 339−367.

(13) Mouesca, J.-M.; Noodleman, L.; Case, D. A.; Lamotte, B. *Inorg. Chem.* **1995**, *34*, 4347.

**Table 11.** Present Classification of the Different Oxidized and Reduced Centers, in Synthetic Analogues and Proteins, According to Their Spin States and Localization/Delocalization of Their Mixed-Valence Pairs

| $[4Fe-4S]^{3+}$ centers | | | $[4Fe-4S]^{+}$ centers | | |
|---|---|---|---|---|---|
| designation | spin state | loc/deloc | designation | spin state | loc/deloc |
| center I | $\|^9/_2,4,^1/_2\rangle$ | localized? | center $I_R$ | $\|^7/_2,3,^1/_2\rangle$ | delocalized |
| center III | $\|^7/_2,3,^1/_2\rangle$ | delocalized | center 8 | $\|^9/_2,4,^1/_2\rangle$ | localized |
| center IV | $\|^7/_2,3,^1/_2\rangle$ | delocalized | aconitase | $\|^9/_2,4,^1/_2\rangle$ | delocalized |
| $HiPIP_{ox}$ | $\|^7/_2,3,^1/_2\rangle$ | delocalized | $Fd_{red}$ | $\|^7/_2,3,^1/_2\rangle$ | delocalized |

the spin state of the system as being, within a pairwise coupling scheme, $|S_{mv},S_{ferrous},S_{total}\rangle = |^9/_2,4,^1/_2\rangle$. Moreover, the mixed-valence pair appears as being *localized.* A finer analysis of the results (notably the eigenvalues and eigenvectors associated with the anisotropic tensors, and the distribution of the error function among the protons) revealed that, upon reduction of the anion, the nearest cation most probably has approached to the paramagnetic center by about 0.4 Å (see Table 9), adopting two very close positions, clearly distinguishable upon examining the corresponding ENDOR lines.

JA963350N